

Development

Granule Cells Constitute One of the Major Neuronal Subtypes in the Molecular Layer of the Posterior Cerebellum

Moushumi R. Dey, Kirthan Reddy, Hiroichi Yoshida, Naoko Nishiyama,  Boris V. Zemelman, and  Hiroshi Nishiyama

<https://doi.org/10.1523/ENEURO.0289-21.2022>

Center for Learning and Memory, Department of Neuroscience, The University of Texas at Austin, Austin, TX 78712

Abstract

The migration of neurons from their birthplace to their correct destination is one of the most crucial steps in brain development. Incomplete or incorrect migration yields ectopic neurons, which cause neurologic deficits or are negligible at best. However, the granule cells (GCs) in the cerebellar cortex may challenge this traditional view of ectopic neurons. When animals are born, GCs proliferate near the pia mater and then migrate down to the GC layer located deep in the cerebellar cortex. However, some GC-like cells stay in the molecular layer, a layer between the pia mater and GC layer, even in normal adult animals. These cells were named ectopic GCs nearly 50 years ago, but their abundance and functional properties remain unclear. Here, we have examined GCs in the molecular layer (mGCs) with a specific marker for mature GCs and transgenic mice in which GCs are sparsely labeled with a fluorescent protein. Contrary to the previous assumption that mGCs are a minor neuronal population, we have found that mGCs are as prevalent as stellate or basket cells in the posterior cerebellum. They are produced during a similar period as regular GCs (rGCs), and *in vivo* time-lapse imaging has revealed that mGCs are stably present in the molecular layer. Whole-cell patch-clamp recordings have shown that mGCs discharge action potentials similarly to rGCs. Since axonal inputs differ between the molecular layer and GC layer, mGCs might be incorporated in different micro-circuits from rGCs and have a unique functional role in the cerebellum.

Key words: cerebellum; development; ectopic neurons; granule cells; migration

Significance Statement

During brain development, neurons migrate away from the place they are born to their correct destination. A defect in this process yields ectopic neurons, i.e., abnormally positioned neurons, which have been considered harmful and studied mostly in the context of brain diseases. Here, we show that abundant granule cells (GCs) in the cerebellum are located ectopically in normal, healthy animals. These neurons are functionally mature and discharge action potentials similarly to conventional GCs. The seemingly ectopic GCs in the normal cerebellum may not be harmful or negligible. Rather, their abundance and distinct location suggest that they might play a unique functional role in the cerebellum via previously unconsidered neuronal connections.

Introduction

Neuronal migration is an elaborate developmental program, and a failure in this process often causes severe motor and cognitive dysfunction because of brain malformation.

Therefore, ectopic neurons, abnormally positioned neurons, have been studied mostly in their relation to neurologic diseases (Takao et al., 2001; Pierce et al., 2005; McCloskey et

Author contributions: M.R.D. and H.N. designed research; M.R.D., K.R., N.N., and H.N. performed research; B.V.Z. contributed unpublished reagents/analytic tools; M.R.D., K.R., H.Y., and H.N. analyzed data; M.R.D. and H.N. wrote the paper.

Received July 3, 2021; accepted April 18, 2022; First published May 18, 2022.

The authors declare no competing financial interests.

al., 2006; Watrin et al., 2015). However, some neurons are placed ectopically even in the normal, healthy brain. Well-known examples are granule cells (GCs) in the hippocampal dentate gyrus (DG) and cerebellar cortex (Chan-Palay, 1972; Palay and Chan-Palay, 1974; Gaarskjaer and Laurberg, 1983; Scharfman et al., 2007). These seemingly harmless ectopic neurons have not been paid much attention, and it remains largely unclear whether they are just tolerable errors or play some roles in brain function.

The mature cerebellar cortex consists of four distinct layers: the molecular layer, Purkinje cell layer, GC layer, and white matter in this order from the surface (Palay and Chan-Palay, 1974; Altman and Bayer, 1996). GCs migrate down from the surface to the GC layer during development, but some GCs have been found in the molecular layer of the normal adult cerebellum in various animal species (Brzustowicz and Kernohan, 1952; Spacek et al., 1973; Palay and Chan-Palay, 1974; Lafarga and Berciano, 1985; Berciano and Lafarga, 1988).

Thus far, those molecular layer GCs (mGCs) have been studied using nonspecific histochemical techniques, such as hematoxylin-eosin staining and Nissl staining. With these staining techniques, mGCs can be unambiguously identified only when they form a clear, distinguishable cluster near the pia mater. If individual mGCs are dispersed throughout the molecular layer, they are difficult to identify because their staining pattern appears similar to that of molecular layer interneurons (MLIs), i.e., stellate cells and basket cells. As a consequence, the number of mGCs has likely been underestimated. Indeed, Golgi staining revealed GCs distributed throughout the molecular layer (Lafarga and Berciano, 1985; Berciano and Lafarga, 1988). Although Golgi staining is nonspecific, it highlights the entire structure of sparsely labeled cells, allowing cell-type identification. The dendritic structure of mGCs is slightly different from regular GCs in the GC layer (rGCs); hence they were considered immature forms of GCs (Lafarga and Berciano, 1985). Combined with the assumption that GCs are a minor population in the molecular layer, mGCs have been regarded as a harmless error in migration (Berciano and Lafarga, 1988).

It may be too early to draw such a conclusion because previous studies of mGCs were performed several

decades ago before a GC-specific marker was established. Therefore, the actual abundance of mGCs remains unclear. Furthermore, the functional properties of mGCs have not yet been studied because identifying them in living tissues was nearly impossible. Now, the GABA_A receptor $\alpha 6$ subunit (GABA_AR $\alpha 6$) is an established marker for mature GCs (Kato, 1990; Laurie et al., 1992b; Nusser et al., 1996; Mellor et al., 1998). A transgenic mouse line in which GCs are selectively labeled with fluorescent proteins is available for functional characterization of mGCs (Huang et al., 2013; Shima et al., 2016; Dhar et al., 2018). Using these new tools, we have found that mGCs, GABA_AR $\alpha 6$ -positive cells, are as prevalent as stellate or basket cells in the molecular layer of the posterior cerebellum. Whole-cell patch-clamp recordings and *in vivo* time-lapse imaging suggest that mGCs are stable components in the molecular layer, potentially participating in local synaptic circuitry in a different way from rGCs.

Materials and Methods

Animals

C57BL/6J (B6) mice and TCGO transgenic mice (males and females) were used for this study. TCGO is one of >200 enhancer trap lines that label small subsets of neurons (Shima et al., 2016). A fraction of cerebellar GCs expresses mCitrine fluorescent protein in TCGO mice (Huang et al., 2013; Dhar et al., 2018), although it is unknown why mCitrine expression is GC-specific and why the labeling is sparse. TCGO line was backcrossed to B6, and the experimental animals were obtained from TCGO \times B6 and TCGO \times TCGO. The mice were four-month-old or older unless otherwise stated. All animal procedures were performed in accordance with the University of Texas at Austin, Institutional Animal Care and Use Committee's regulations.

5-Bromo-2'-deoxyuridine (BrdU) cell proliferation assay

BrdU was subcutaneously injected into B6 pups (150 mg/kg). Individual pups received two pulses of injection (4-h interval) either at postnatal day (P)4, P8, or P12 and were returned to the home cage with their mother. They were sacrificed approximately two months after the injection and processed for immunohistochemistry as described below but with an additional antigen retrieval step. For antigen retrieval, cerebellar sections were first incubated with 2N HCl at room temperature for 30 min. The HCl was washed thoroughly with PBS (in mM; 137 NaCl, 2.7 KCl, 8 Na₂HPO₄, and 2 KH₂PO₄, pH 7.4) containing 0.5% Triton X-100 (PBST) before proceeding to the blocking step of immunohistochemistry. Image acquisition and analysis were performed as described below.

Immunohistochemistry

B6 or TCGO mice were anesthetized with an intraperitoneal injection of ketamine/xylazine (100/10 mg/kg) and then intracardially perfused with 4% paraformaldehyde in PBS. The brains were extracted postperfusion and immersed in the same fixative overnight at 4°C. After washing the tissues with PBS, sagittal sections of the

This work was supported by National Institutes of Health Grants NS073919 (to H.N.) and NS094330 (to B.V.Z.) and by the McKnight Memory and Cognitive Disorders Award (B.V.Z.).

Acknowledgement: We thank Adam Hantman for providing the TCGO transgenic mice; Daniel Johnston, Richard Gray, and Darrin Brager for helpful support to conduct electrophysiology experiments; and Michael Drew for advice in BrdU cell proliferation assay.

M. R. Dey's present address: Department of Cellular and Integrative Physiology, The University of Texas Health Science Center at San Antonio, San Antonio, TX 78229.

K. Reddy's present address: McGovern Medical School, The University of Texas Health Science Center at Houston, Houston, TX 77030.

Correspondence should be addressed to Hiroshi Nishiyama at hiroshi@utexas.edu.

<https://doi.org/10.1523/ENEURO.0289-21.2022>

Copyright © 2022 Dey et al.

This is an open-access article distributed under the terms of the Creative Commons Attribution 4.0 International license, which permits unrestricted use, distribution and reproduction in any medium provided that the original work is properly attributed.

cerebellum (30–60 μm in thickness) were cut using Microm HM650V vibration microtome (Thermo Fisher Scientific). The sections were washed with PBST and blocked for at least 1 h at room temperature in PBST containing 5% normal donkey serum. Following the blocking step, the sections were incubated with primary antibodies overnight at 4°C, then washed with PBST and incubated with secondary antibodies for at least 2 h at room temperature. Sections were then washed with PBST and mounted with mounting media (Fluoromount-G, SouthernBiotech). The list of the primary and secondary antibodies is shown below.

Primary antibodies: anti-GABA_AR α 6 rabbit polyclonal antibody (1:500, #224603, Synaptic Systems), anti-parvalbumin (PV) mouse monoclonal antibody (1:2000, ab277625, Abcam), anti-BrdU rat monoclonal antibody (1:500, ab6326, Abcam), anti-NG2 rabbit polyclonal antibody (1:500, AB5320, Millipore Sigma). Secondary antibodies: donkey anti-rabbit IgG H&L Alexa Fluor 488 (1:500, ab150073, Abcam), donkey anti-mouse IgG H&L Alexa Fluor 568 (1:500, ab175472, Abcam), donkey anti-rat IgG H&L Alexa Fluor 568 (1:500, ab175475, Abcam), donkey anti-rabbit IgG H&L Alexa Fluor 647 (1:500, ab150075, Abcam), donkey anti-mouse IgG H&L Alexa Fluor 647 (1:500, ab150107, Abcam).

Two-color detection was performed with the following fluorophore combination: GABA_AR α 6 (Alexa Fluor 488) – PV (Alexa Fluor 568), GABA_AR α 6 (Alexa Fluor 488) – BrdU (Alexa Fluor 568), mCitrine – GABA_AR α 6, PV, or NG2 (Alexa Fluor 647).

Image acquisition and analysis

The immunostained sections were imaged using Olympus FV1000 laser-scanning confocal microscope (Olympus). Z-stack images were acquired with a 40 \times water immersion objective lens (0.8 NA) at 1- to 1.5- μm step size with the x-y resolution of 0.4–0.6 $\mu\text{m}/\text{pixel}$. Alexa Fluor 488 and Alexa Fluor 568 were excited by 488- and 543-nm lasers, respectively. The green (Alexa Fluor 488) and orange (Alexa Fluor 568) fluorescent emissions were separated by a long-pass filter 560 nm and then filtered by bandpass filters 505–525 and 560–660 nm, respectively. mCitrine and Alexa Fluor 647 were excited by 515- and 635-nm lasers, respectively. The yellow (mCitrine) and red (Alexa Fluor 647) fluorescent emissions were separated by a long-pass filter 640 nm and then filtered by bandpass filters 535–565 and 655–755 nm, respectively. The laser intensity and the sensitivity of the photomultiplier tubes were manually optimized in each field of view (FOV) because the signal intensity and background noise are not always the same across samples and even within a sample.

To quantify the density of mGCs and MLIs (the mixture or basket and stellate cells) in B6 mice, the number of GABA_AR α 6-positive cells (mGCs) and PV-positive cells (MLIs) were manually counted in 3D, z-stack images. The FOVs were selected from the anterior lobe (Lobules I–V), posterior lobe (Lobules VI–IX), and flocculonodular lobe (Lobule X). Then, in each FOV, the numbers of mGCs and MLIs were divided by the ML volume to obtain the density. The ML volume (range; $5.8 \times 10^{-4} \text{ mm}^3$ to $28.0 \times 10^{-4} \text{ mm}^3$) was calculated as the ML area \times the depth of the z-stack in which counted cells were included. The

numbers of animals and FOVs in each lobe are shown in Figure 1 legend.

For BrdU cell proliferation assay in B6 mice, the numbers of GABA_AR α 6-positive cells and BrdU/GABA_AR α 6-double-positive cells were manually counted in the molecular layer and GC layer in 3D, z-stack images. Then, the fraction of BrdU/GABA_AR α 6-double-positive cells in GABA_AR α 6-positive cells was calculated in each layer. The FOVs were selected randomly from the entire cerebellum. The numbers of animals and FOVs are shown in Figure 2 legend. The average volume for quantification was $14.0 \times 10^{-4} \text{ mm}^3$. The quantification was done by two experimenters, one knew when BrdU was injected, and the other did not.

For the identification of mCitrine-expressing cells, at least four TCGO mice were used for each immunostaining against GABA_AR α 6, PV, or NG2. The FOVs were selected randomly from the entire cerebellum, and the images were examined whether the immunoreactivity colocalized with mCitrine fluorescence.

Cranial window preparation

TCGO mice (one month old or older) were anesthetized with 5% isoflurane, and the dose was reduced to 1.5–2% following the induction. A cranial window was created on the dorsal surface of the cerebellar cortex (Lobules VI–VIII) as described in a previous study (Nishiyama et al., 2014). Briefly, the scalp, muscles, and fascia overlying the skull were removed. A small metal bar (12 \times 2 mm in length and \sim 0.9 mm in thickness) was glued to the skull near the lambda with surgical cyanoacrylate (Vetabond, 3M) and dental cement (Ortho-Jet, Lang Dental). The mouse's head was stabilized by clamping the metal bar to the surgical stage. A dental drill and a small drill bit (0.5-mm tip diameter) were used for etching a rectangular (\sim 2 \times 1.5 mm) craniotomy on the skull. After an opening was made, a coverslip was placed directly on top of the dura and secured in place using the surgical cyanoacrylate and dental cement. The animal was then allowed to recover from the anesthesia and returned to the home cage. Carprofen (5 mg/kg) was administered for 2 d postsurgery as an analgesic.

In vivo time-lapse imaging

We began long-term two-photon *in vivo* time-lapse imaging one to two weeks after the cranial window preparation. Mice were lightly anesthetized with 1–1.5% isoflurane and securely positioned on a custom-made x-y translator under Olympus FV1000 two-photon laser-scanning microscope (Olympus). mCitrine was excited by 920-nm pulsed infrared laser provided by Mai Tai HP DeepSee mode-locked Ti:sapphire laser (Spectra-Physics). The emitted fluorescence was collected with a 25 \times water immersion objective lens (1.05 NA) and detected by an external gallium arsenide photodetector (GaAsPs; Hamamatsu).

Both mGCs and rGCs express mCitrine in TCGO mice. However, mGCs and rGCs are unambiguously distinguishable because mGCs are found within parallel fiber bundles, which exist only in the molecular layer. Z-stack images (1.5- μm step size, 30–60 planes with the x-y

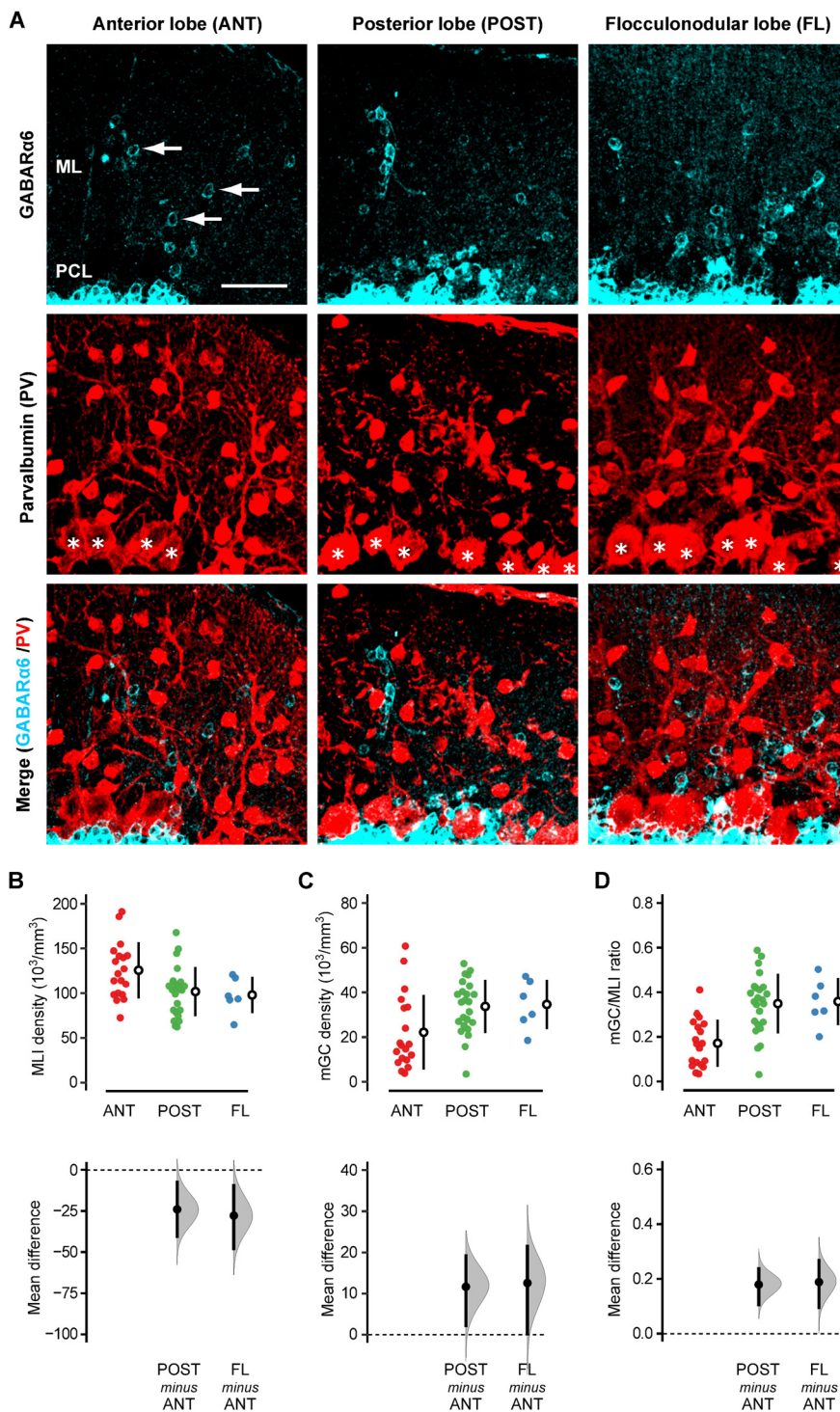


Figure 1. Immunohistochemical detection of mGCs and MLIs. **A**, The sagittal cerebellar slices of B6 mice were double-stained with antibodies for GABA α R α 6 (cyan, top row) and PV (red, middle row). The merged images are shown in the bottom row. Note that GABA α R α 6 signals do not colocalize with the somata of PV-positive cells. The left, middle, and right columns show examples taken from the anterior lobe (ANT; Lobules I–V), posterior lobe (POST; Lobules VI–IX), and flocculonodular lobe (FL; lobule X), respectively. The arrows in the top row indicate examples of mGCs. The asterisks in the middle row indicate Purkinje cell somata. ML, molecular layer; PCL, Purkinje cell layer. Scale bar: 40 μm . **B–D**, The density of MLIs (**B**), mGCs (**C**), and the mGC/MLI ratio (**D**) were quantified in each lobe, and the mean differences between ANT versus POST and ANT versus FL were estimated by bootstrap resampling. In the top panels, the closed circles indicate individual FOVs taken from ANT (red; $n = 19$), POST (green; $n = 24$), and FL (blue; $n = 6$) of four mice. The open circles and vertical lines indicate the mean and standard deviation (SD), respectively. In the bottom panels, the gray curves indicate the resampled distribution of the mean difference between ANT versus POST (POST minus ANT) and ANT versus FL (FL minus ANT). The closed black circles and vertical lines indicate the observed mean difference and 95% confidence

continued

interval, respectively. The horizontal dashed line is the line of zero mean difference. The statistical significance ($p < 0.05$) is assessed whether the 95% confidence interval includes this zero-line or not. Furthermore, the sharpness of the resampled distribution (relative to the mean difference) and the proximity of the confidence interval to the zero-line allow us to infer the certainty of the difference. All the estimation graphics used in this study have the same structure.

resolution of $0.3 \mu\text{m}/\text{pixel}$) were taken repetitively in the same FOVs once a week until the window clarity diminished or the animals showed a sign of potential health concern. The brain surface vasculature was used to locate the same FOVs roughly, and the position was confirmed and refined by mGC signals, which were stable across time points. We imaged 344 mGCs from 17 mice in total. Among them, 181 mGCs from 10 mice were imaged longer than one month. Since the inability of month-long imaging likely reflects suboptimal surgery, we only focused on those 181 mGCs and tracked their presence in 3D z-stacks across timepoints. Cells located near the top or bottom of a z-stack were excluded from the analysis because those cells might not be captured at every time point because of a slight angular difference in the optical axis.

Electrophysiology

TCGO mice were deeply anesthetized with isoflurane. The cerebellum was quickly removed after decapitation and submerged in an ice-cold cutting solution containing (in mM): 2.5 KCl, 0.5 CaCl_2 , 7.0 MgCl_2 , 1.25 NaH_2PO_4 , 25 NaHCO_3 , 205 Sucrose, and 15 glucose bubbled with 95% O_2 and 5% CO_2 . Parasagittal slices ($200 \mu\text{m}$ thick) were cut using a 7000smz-2 vibration microtome (Campden Instruments), recovered in artificial CSF (ACSF; in mM: 125 NaCl, 2.5 KCl, 1.25, NaH_2PO_4 , 25 NaHCO_3 , 2 CaCl_2 , 1 MgCl_2 , and 10 glucose) for 30 min at 32°C , and then stored at room temperature until used for recording. Recordings were performed at 32°C .

Whole-cell patch-clamp recordings were made using Multiclamp 700B amplifier (Molecular Devices) and AxoGraph data acquisition software (AxoGraph). The tip of the recording pipettes ($7\text{--}12 \text{ M}\Omega$) was wrapped with Parafilm to reduce the capacitance. Whole-cell current-clamp recordings were performed using the pipettes filled with the intracellular solution containing (in mM): 150 K-gluconate, 10 NaCl, 10 K-HEPES, 3 $\text{Na}_2\text{-ATP}$, 0.3 Na-GTP (305–310 mOsm, pH adjusted to 7.3 with KOH). mCitrine-expressing cells in the molecular layer (mGC+), mCitrine-expressing cells in the GC layer (rGC+), and mCitrine-nonexpressing cells in the GC layer (rGC–) were selected at random, but mGC+ located at the pia mater was avoided. Series resistance was compensated using bridge balance, and pipette capacitance was neutralized. Cells that required $>1.5 \text{ pF}$ of capacitance neutralization were removed from further analysis. Passive and active membrane properties of the cells were quantified as described below.

Electrophysiology data analysis

Hyperpolarizing current steps (750 ms, $1\text{--}10 \text{ pA}$ with 1-pA increment) were injected to quantify resting membrane

potentials and input resistance. Resting membrane potentials were obtained as the averaged voltages without holding current. To quantify input resistance, the steady-state voltage deflection by each hyperpolarizing current was obtained as the averaged voltage during the last 200 ms of hyperpolarizing current injection. The voltage deflections were plotted as the function of the amplitude of the injected currents, and input resistance was obtained as the slope of the linear regression line.

Depolarizing current steps (750 ms, $0\text{--}35 \text{ pA}$ with 5-pA increment) were injected to quantify the excitability of the cells. Action potential threshold was obtained as the voltage where dV/dt exceeds 10 mV/ms . The action potential firing frequency was obtained as the mean firing rate during the first 200-ms period of depolarizing current injection. Input threshold was defined as the minimum current that elicited action potentials. The action potential frequencies were plotted as the function of the amplitude of the injected currents, and the linear regression line was obtained within the domain from the maximum current that did not elicit action potentials and 35 pA . The slope of this line was used as a measure of the input-output relationship.

The measurements were performed with AxoGraph, and the obtained data were processed with custom-written R codes for visualization, linear fit, and statistical analysis.

Statistical analysis

Bootstrap resampling (5000 resamples) was performed using an R package dabestr (Ho et al., 2019) to present the effect size, i.e., the mean difference between control and test groups, with its resampling distribution and 95% confidence interval. If the 95% confidence interval does not include zero, it is equivalent to $p < 0.05$ in null hypothesis significance testing. This method does not require the sample or population to be normally distributed. Furthermore, showing the effect size with its entire range of distribution allows better inference beyond whether the effect is statistically significant or not (Calin-Jageman and Cumming, 2019; Ho et al., 2019).

Regarding passive and active membrane properties, mGC+ showed a smaller variance than rGC+ and rGC– in the input resistance and current-frequency (input-output) relationship. Bartlett's test was used in these cases to test the homogeneity of variance, and $p < 0.05$ was considered statistically significant.

Results

GC is one of the major neuronal subtypes in the molecular layer of the posterior cerebellum

According to the traditional view of cerebellar anatomy, MLIs (basket cells and stellate cells) are the only neuronal subtypes that have their somata in the

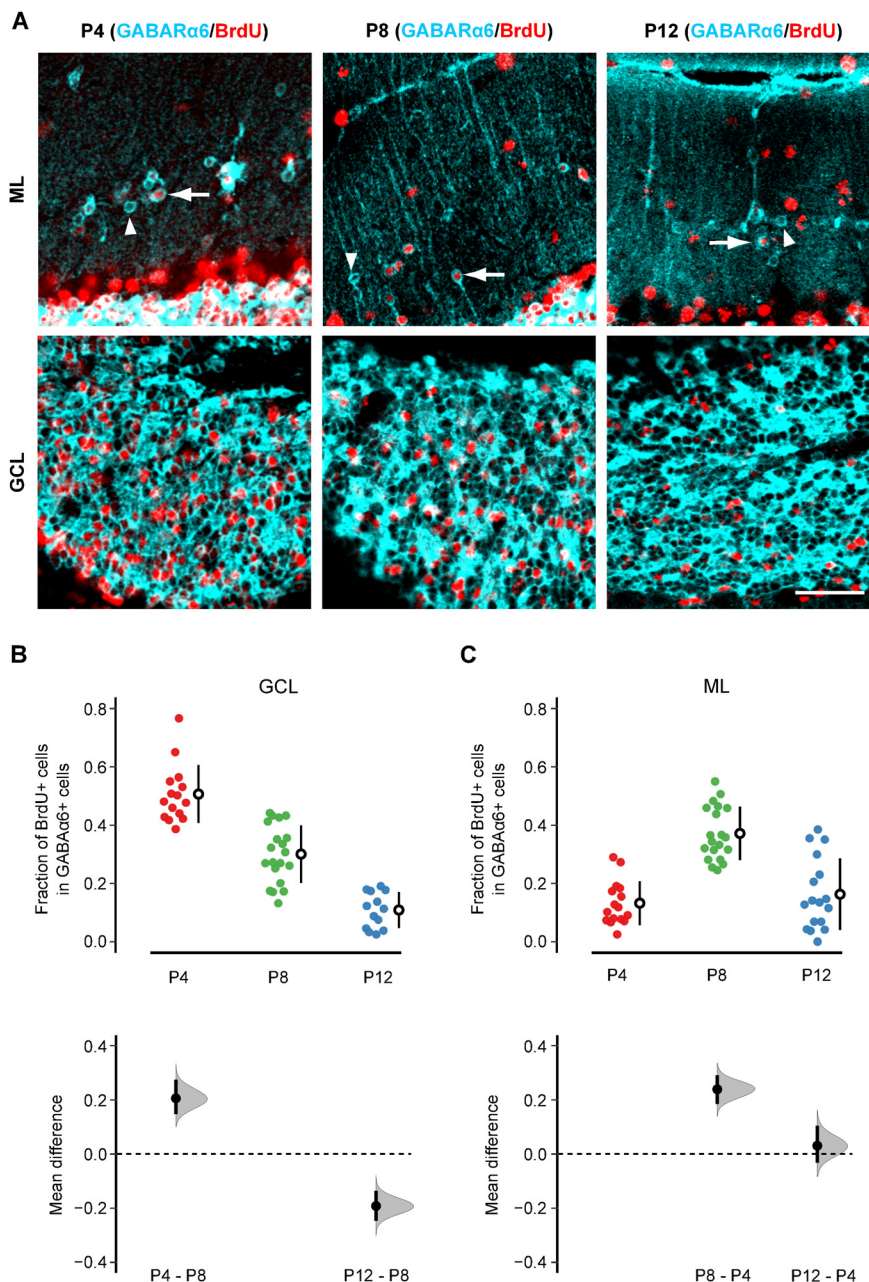


Figure 2. BrdU cell proliferation assay. **A**, Representative images of BrdU (red) and GABA_ARα6 (cyan) double staining in the normal adult cerebellum. The top and bottom rows indicate the images taken from the molecular layer (ML) and GC layer (GCL), respectively. BrdU was injected at P4 (left column), P8 (middle column), or P12 (right column). The arrows indicate examples of BrdU-positive mGCs, whereas the arrowheads indicate examples of BrdU-negative mGCs. Scale bar: 40 μ m. **B**, **C**, The fraction of BrdU-positive cells in GABA_ARα6-positive cells was quantified in the GCL (**B**) and ML (**C**), and the mean differences between the BrdU injection days were estimated by bootstrap resampling. In the top panels, the closed circles indicate individual FOVs obtained from P4 injection (red; $n = 15$ for GCL, 16 for ML from 4 mice), P8 injection (green, $n = 20$ for GCL, 20 for ML from 5 mice), and P12 injection (blue; $n = 13$ for GCL, 17 for ML from 4 mice). The open circles and vertical lines indicate the mean and SD, respectively. In the bottom panels, the estimated mean differences between P8 versus P4 (P4 – P8) and P8 versus P12 (P12 – P8) are shown for the GCL (**B**), and the estimated mean differences between P4 versus P8 (P8 – P4) and P4 versus P12 (P12 – P4) are shown for the ML (**C**). The gray curves indicate the resampled distribution of the mean difference. The closed black circles and vertical lines indicate the observed mean difference and 95% confidence interval, respectively. The horizontal dashed line is the line of zero mean difference.

molecular layer (Palay and Chan-Palay, 1974; Altman and Bayer, 1996; D'Angelo, 2018). Therefore, we first performed double-immunohistochemistry using the anti-GABA_ARα6 antibody and anti-parvalbumin (PV) antibody

to quantify how prevalent GCs are, relative to MLIs, in the molecular layer of B6 mice.

GCs express GABA_A receptors and the subunit expression pattern changes with developmental stages; GC

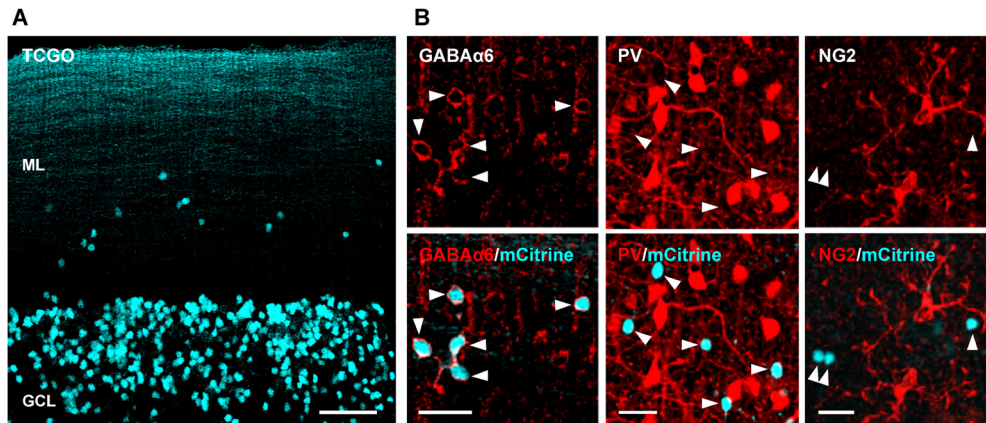


Figure 3. mCitrine exclusively labels mGCs in the molecular layer of TCGO mice. **A**, The cerebellar cortex of TCGO mice. mCitrine-expressing cells (cyan) are seen in the molecular layer (ML) and GCs layer (GCL). Scale bar: 50 μm . **B**, The molecular layer of TCGO mice was immunostained with antibodies for GABA α 6 (left column), PV (middle column), or NG2 (right column). The merged images (bottom row) show the mCitrine signal and the antibody signal in cyan and red, respectively. The arrowheads indicate the location of mCitrine-expressing cells. Note that mCitrine-expressing cells are co-labeled only with the anti-GABA α R α 6 antibody. Scale bar: 20 μm .

precursors express the subunits α 2, α 3, β 3, γ 1, and γ 2, whereas the expression of the subunit α 6 (GABA α R α 6) is restricted to postmigratory mature GCs (Laurie et al., 1992a). Therefore, GABA α R α 6 has been used as a marker for mature GCs (Kato, 1990; Laurie et al., 1992b; Nusser et al., 1996; Mellor et al., 1998).

PV, a slow calcium-binding protein, is expressed in subsets of GABAergic interneurons, and its expression is specific to MLIs, Golgi cells, and Purkinje cells in the cerebellar cortex (Bastianelli, 2003). Among them, Golgi cells are located in the GC layer, and Purkinje cells are located at the bottom of the molecular layer. Within the molecular layer, anti-PV antibody labels Purkinje cell dendrites, but it highlights the soma of MLIs (Fig. 1A, middle). Therefore, it has been used to label MLIs in various animal species (Ohshima et al., 1991; Kadowaki et al., 1993; Fortin et al., 1998; Kalinichenko and Pushchin, 2008; Kamiya and Sawada, 2021).

The anti-GABA α R α 6 antibody labeled GCs as small, open circles in the molecular layer (Fig. 1A, top), which were distinct from PV-positive MLIs (Fig. 1A, bottom). We called them mGCs and quantified the density of mGCs, MLIs, and their ratio (mGC/MLI) on parasagittal sections of the cerebellar vermis.

The cerebellum is divided into three lobes along the anterior-posterior axis by two major fissures: the anterior lobe (Lobules I–V), posterior lobe (Lobules VI–IX), and flocculonodular lobe (Lobule X). The density of mGCs and MLIs varied across the FOVs in all three lobes. However, as a population, the anterior lobe had more MLIs ($125.7 \pm 31.5 \times 10^3/\text{mm}^3$, mean \pm SD) and fewer mGCs ($22.2 \pm 16.7 \times 10^3/\text{mm}^3$) than the posterior lobe (MLIs: $101.8 \pm 27.4 \times 10^3/\text{mm}^3$, mGCs: $33.8 \pm 11.9 \times 10^3/\text{mm}^3$) and flocculonodular lobes (MLIs: $98.0 \pm 20.2 \times 10^3/\text{mm}^3$, mGCs: $34.7 \pm 11.0 \times 10^3/\text{mm}^3$). Figure 1B,C shows these results (top panels) with the mean difference between the anterior lobe and other lobes, with its estimated distribution and 95% confidence interval (bottom panels). Except

for the difference in mGC density between the anterior lobe and flocculonodular lobe (Fig. 1C, bottom right), these differences were statistically significant, i.e., the 95% confidence interval of the mean difference not including zero. However, even in these statistically significant cases, the 95% confidence intervals contain values close to zero, suggesting that the actual difference could be minimal or uncertain.

The primary purpose of this analysis is to quantify the relative abundance of GCs as compared with MLIs. Therefore, we calculated the mGC/MLI ratio in each FOV (Fig. 1D). The ratio was significantly higher in the posterior lobe (0.35 ± 0.13) and the flocculonodular lobe (0.36 ± 0.11) than the anterior lobe (0.17 ± 0.11). Furthermore, the 95% confidence interval was narrow relative to the mean difference, suggesting that the difference is likely real.

It is important to note that MLIs are a mixture of two different neuronal types: basket cells and stellate cells. If the mGC/MLI ratio is 0.35, and the number of basket cells and stellate cells are comparable, the ratio of mGC: basket: stellate is estimated to be $0.35:0.5:0.5 = 0.7:1:1$. Therefore, the number of mGCs is estimated to be $\sim 70\%$ of each MLI subtype in the posterior cerebellum.

mGCs are produced during a similar period as rGCs

When animals are born, GCs proliferate near the pia mater and form the external GC layer (Rahimi-Balaei et al., 2018). The external GC layer then gradually disappears as postproliferating GCs migrate down through the molecular layer to form the GC layer deep inside the cortex (Altman and Bayer, 1996; Rahimi-Balaei et al., 2018). Although mGCs are speculated to be the last ones to exit the mitotic cycle and thus could not complete their migration to the GC layer (Lafarga and Berciano, 1985), no previous study has tested this hypothesis. Therefore, we performed BrdU cell proliferation assay combined with GABA α R α 6 immunostaining to test whether

mGCs represent the group of GCs that exit the mitotic cycle last (Fig. 2).

We injected BrdU into B6 pups at P4, P8, or P12. These dates were chosen because P4–P12 covers the almost entire range of GC proliferation as previous studies showed that the fraction of proliferating GCs was nearly 100% at P4, ~50% at P8, and only 10–20% at P12 in rats (Fujita, 1967). We sacrificed the mice two months after the BrdU injection and double-stained the sections with anti-BrdU antibody and anti-GABA_ARα6 antibody (Fig. 2A). Then, the fraction of BrdU-positive cells in the population of GABA_ARα6-positive cells was quantified in each FOV without distinguishing lobes (Fig. 2B, C). We did not address potential differences among lobes for the rest of this study.

The fraction of BrdU-positive GCs, i.e., BrdU and GABA_ARα6-double-positive cells, showed a steady decline in the GC layer as BrdU was injected at a later time point (Fig. 2B). It indicates that our BrdU cell proliferation assay reliably captured the overall time course of GC proliferation. Therefore, this assay can be used to examine the time course of mGC production.

If mGCs are the last group of GCs that exit the mitotic cycle, all of them should be labeled by BrdU regardless of the timing of injection. In this scenario, two possible outcomes are expected. One possibility is that the fraction of BrdU-positive GCs is not affected by the timing of BrdU injection in the molecular layer. However, it is reasonable to assume that the strength of BrdU labeling gradually decreases and eventually becomes undetectable as cells undergo more mitotic cycles after the BrdU injection. Therefore, the other possibility is that the fraction of BrdU-positive GCs increases in the molecular layer as injection timing is delayed toward the end of the GC proliferation phase. As shown in Figure 2C, the experimental outcome was different from both of these predictions. The average fraction of BrdU-positive GCs was highest in the molecular layer when BrdU was injected at P8 (0.37 ± 0.09), which was more than twice as P4 (0.13 ± 0.07) and P12 (0.16 ± 0.12) injections (Fig. 2C, top). The mean difference between P4 and P8 injection was significant with the narrow confidence interval relative to the difference, whereas there was no significant difference between P4 and P12 injection (Fig. 2C, bottom). These results indicate that mGCs are not merely the last group of GCs that exit the mitotic cycle. Thus, although mGC production may be slightly delayed from regular GCs in the GC layer (rGCs), the timing of mGC production appears to be largely overlapped with rGC production.

mGCs are stable components of the cerebellar cortex

It is yet to be known whether mGCs are late migrating cells, dying over time because of incorrect placement, or stable components in the molecular layer. To determine which of these possibilities is the case, mGCs must be visualized in living specimens. We, therefore, characterized the transgenic mouse line called TCGO, in which rGCs are labeled by the fluorescent protein mCitrine (Huang et al., 2013; Shima et al., 2016; Dhar et al., 2018). Consistent with the previous report, rGCs were sparsely labeled by

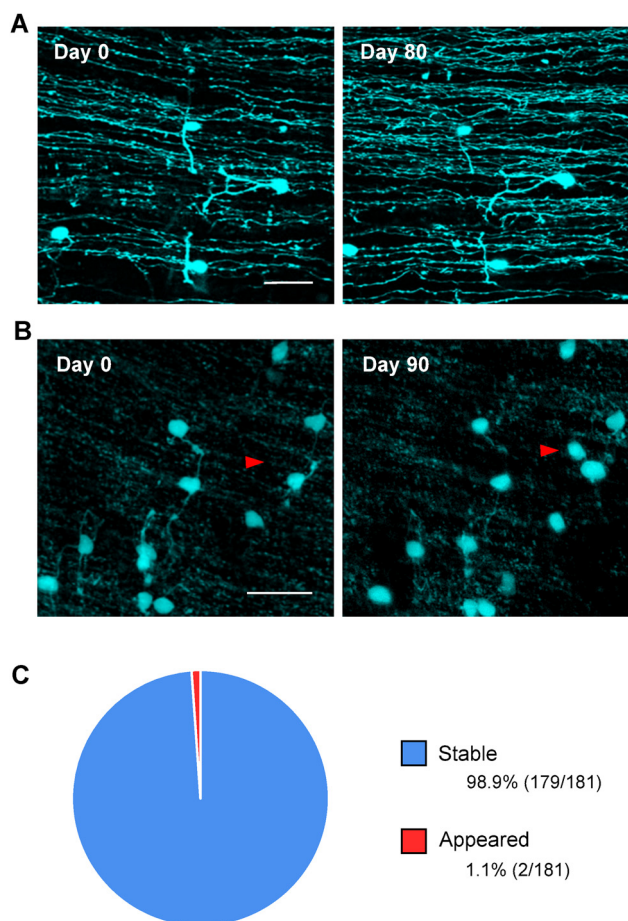


Figure 4. Long-term time-lapse *in vivo* imaging of mGCs. **A, B**, Representative images of mGCs *in vivo*. Images taken on the first day of imaging (day 0) are compared with the image taken 80 d later (**A**) and 90 d later (**B**). Axons running laterally in the images are parallel fibers. Red arrowheads in **B** indicate the mGC that did not exist on day 0 but appeared on day 90. Note that the images are maximum projections; hence, a small angular difference in the optical axis sometimes causes false changes in the projected images. The appearance of the mGC, indicated by the red arrowheads, was confirmed in the z-stack. Scale bar: 20 μ m. **C**, The fractions of stable and newly appeared mGCs were quantified in 181 mGCs (from 10 mice) that were imaged longer than one month. Only two mGCs appeared, and no mGC disappeared. Scale bar: 20 μ m.

mCitrine in TCGO mice (Fig. 3A). Besides, we found mCitrine-expressing cells in the molecular layer as well (Fig. 3A).

To confirm the identity of mCitrine-expressing cells in the molecular layer, we performed immunohistochemistry using antibodies for GABA_ARα6, PV, and NG2, a marker for NG2 glial cells that are known to have their somata in the molecular layer (Levine and Card, 1987; Lin et al., 2005). Only GABA_ARα6 immunosignals colocalize with mCitrine-expressing cells, indicating that they are mGCs, not MLIs or NG2 glial cells (Fig. 3B). Because of the sparse labeling nature of TCGO mice, not all mGCs or rGCs express mCitrine. Regardless, the TCGO mouse line provides a powerful experimental tool to characterize mGCs in living specimens.

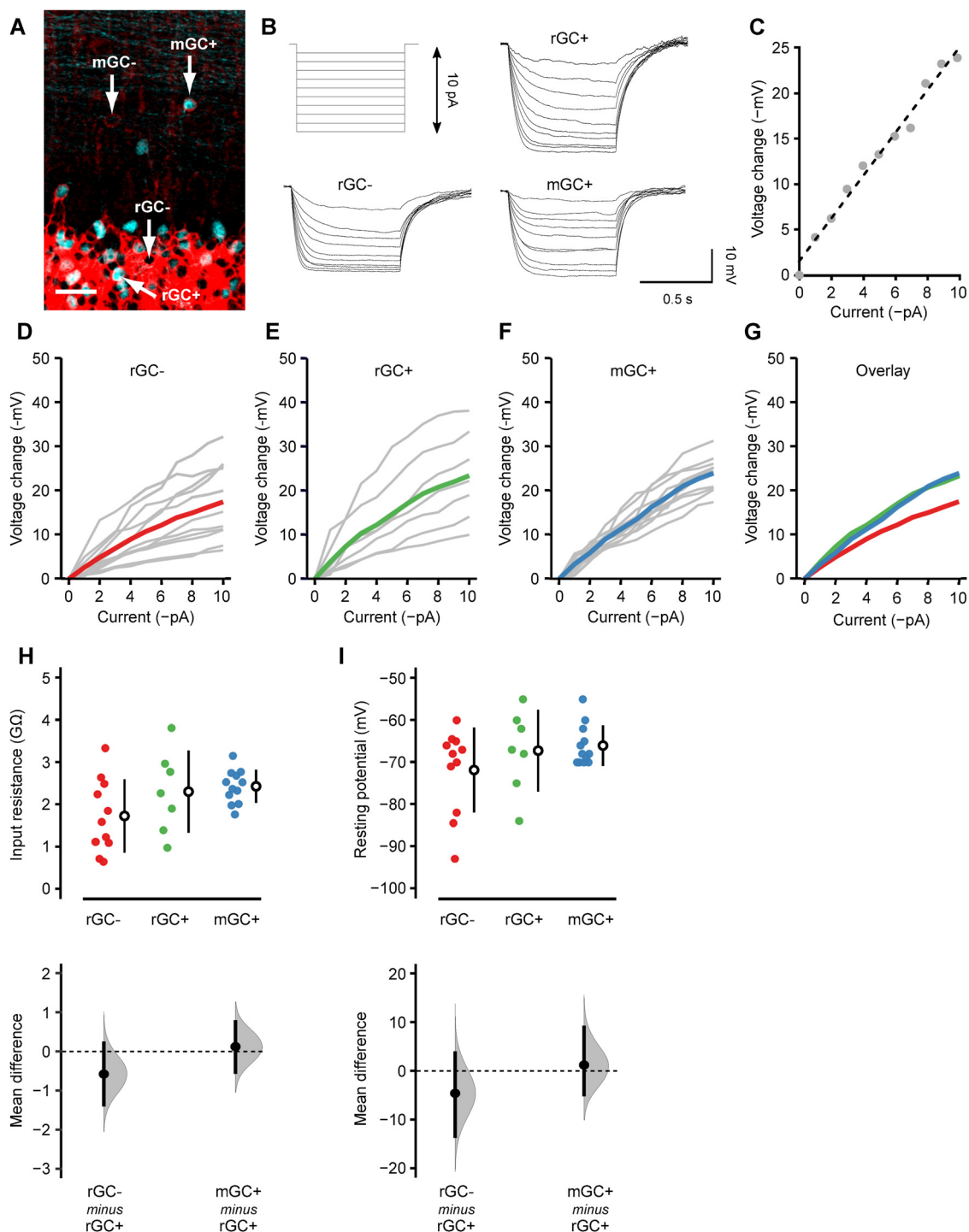


Figure 5. Passive membrane properties of mGCs. **A**, GABA_AR α 6 (red) and mCitrine (cyan) double-labeling in a fixed tissue to show the identity of recorded cells. Whole-cell current-clamp recordings were made from rGC⁻ (mCitrine-nonexpressing rGC), rGC⁺ (mCitrine-expressing rGC), and mGC⁺ (mCitrine-expressing mGC). mGC⁻ (mCitrine-nonexpressing mGC) is invisible in living tissues, thus not recorded. Scale bar: 20 μ m. **B**, Hyperpolarizing current steps (1-pA increment) injected into the cells (top, left) and the resultant membrane hyperpolarization in a rGC⁻ (bottom, left), rGC⁺ (top, right), and mGC⁺ (bottom, right). **C**, A representative current–voltage (I–V) relationship (gray dots) and the linear regression line (dashed line). The input resistance of each cell was obtained as the slope of this linear regression line. **D–F**, The I–V relationship of rGC⁻ (**D**), rGC⁺ (**E**), and mGC⁺ (**F**). Gray lines represent individual cells, and the colored lines represent the population average. **G**, The population averages of rGC⁻ (red), rGC⁺ (green), and mGC⁺ (blue) are overlaid. **H**, **I**, The input resistance (**H**) and resting membrane potential (**I**) of rGC⁻ (red; $n=11$), rGC⁺ (green; $n=7$), and mGC⁺ (blue; $n=12$) were shown, and the mean differences between rGC⁺ versus rGC⁻ and rGC⁺ versus mGC⁺ were estimated by bootstrap resampling. In the top panels, the closed circles indicate individual cells. The open circles and vertical lines indicate the mean and SD, respectively. In the bottom panels, the gray curves indicate the resampled distribution of

continued

the mean difference between rGC+ versus rGC- (rGC- minus rGC+) and rGC+ versus mGC+ (mGC+ minus rGC+). The closed black circles and vertical lines indicate the observed mean difference and 95% confidence interval, respectively. The horizontal dashed line is the line of zero mean difference.

To determine the stability of mGCs, we performed two-photon *in vivo* time-lapse imaging using adult TCGO mice. Since rGCs send their axons, called parallel fibers, to the molecular layer (Altman and Bayer, 1996; Palay and Chan-Palay, 1974); mGCs can be easily identified by their co-presence with parallel fibers (Fig. 4A,B). Among 181 mGCs (from 10 mice) imaged over one month or longer, only two mGCs newly appeared (Fig. 4C). None of the mGCs imaged at the first time point disappeared later. It remains unclear whether the new mGCs actually appeared or mCitrine-nonexpressing mGCs somehow started to express mCitrine. However, almost all mGCs barely changed their positions or shapes, suggesting that they were stable components of the molecular layer.

mGCs discharge action potentials

Because of the uncommon location of mGCs and their morphology, it has been thought that mGCs are erroneous neurons with their maturation stalled midway (Berciano and Lafarga, 1988). However, no functional characterization has yet been made. Using cerebellar slices acutely prepared from TCGO mice, we performed whole-cell patch-clamp recordings from visually identified mGCs. Recordings were made from mCitrine-expressing mGCs (mGC+), mCitrine-expressing rGCs (rGC+), and mCitrine-nonexpressing rGCs (rGC-; Fig. 5A). Although mCitrine-nonexpressing mGCs were not identifiable, thus not recorded, the comparison between rGC+ and rGC- was expected to provide insight into potential differences between mCitrine-expressing and non-expressing GCs, if any.

We held the cells with current-clamp mode and injected a hyperpolarizing current step (0–10 pA) with 1-pA increment (Fig. 5B). The voltage-current relationship was obtained in each cell (Fig. 5C–G), and the input resistance was measured as the slope of the linear regression line (Fig. 5C,H). The input resistance showed substantial cell-to-cell variation in rGC- ($1.65 \pm 0.85 \text{ G}\Omega$) and rGC+ ($2.30 \pm 0.98 \text{ G}\Omega$), as indicated by the relatively large SD compared with the mean. On the other hand, the cell-to-cell variation was small in mGC+ ($2.42 \pm 0.39 \text{ G}\Omega$). The difference in variation was statistically significant ($p = 0.028$, Bartlett's test), suggesting that mGCs are more homogeneous than rGCs.

We also compared the mean input resistance between rGC+ versus rGC- and rGC+ versus mGC+ because rGC+ shares a common property with both cell types (rGC-: location, mGC+: mCitrine expression); thus, suitable as the control group for our statistical analysis. The 95% confidence interval of the mean difference includes zero in both rGC- and mGC+, indicating that the mean input resistance was not significantly different among the cell types (Fig. 5H). The resting membrane potential, measured as the voltage without a holding current, was not significantly different among the cell types either (Fig.

5I). These results suggest that, although mGCs may be more homogenous than rGCs, their passive membrane properties are as mature as rGCs.

We next examined the firing properties of mGCs by injecting a depolarizing current step (0–35 pA) with 5-pA increment (Fig. 6A). All three types of GCs discharged action potentials, and the firing frequency increased as the amplitude of the injected current increased (Fig. 6B–F). Consistent with previous studies (Brandalise et al., 2016), there was substantial cell-to-cell variation in the minimum current required to elicit action potentials (input threshold) and the slope of the current-frequency relationship (Fig. 6G). Similar to the input resistance, mGCs showed the smallest variation in the slope (Fig. 6I), and the difference in variation was statistically significant among the cell types ($p = 0.002$, Bartlett's test). It suggests that the input-output relationship, i.e., how the input strength is converted to the firing frequency, is relatively homogeneous in mGCs. However, there was no significant difference between rGC+ versus rGC- or rGC+ versus mGC+ in the mean input threshold (Fig. 6H), slope (Fig. 6I), or action potential threshold (Fig. 6J) as shown by the 95% confidence interval including zero in all the cases. These results suggest that, although the physiological properties of mGCs may be more homogenous than rGCs, their intrinsic excitability is as mature as rGCs.

Discussions

This study reevaluated mGCs with modern experimental tools that were not available when previous studies characterized them several decades ago. We used the anti-GABA_AR α 6 antibody, a GC-specific marker, to quantify the distribution and abundance of mGCs. We also used the TCGO transgenic mouse line to analyze for the first time the functional properties of mGCs. Our data show that the number of mGCs is estimated to be ~70% of stellate cells or basket cells in the posterior lobe and flocculonodular lobe, and they discharge action potentials in a similar fashion as rGCs. These results suggest that mGCs are one of the major neuronal subtypes in the molecular layer of the posterior cerebellum, potentially forming a previously unconsidered synaptic circuit in the cerebellar cortex.

Quantification of mGCs and MLIs

An anti-GABA_AR α 6 antibody has been used in numerous studies since it was established as a GC-specific marker. But, to our knowledge, those studies barely described mGCs in the normal adult cerebellum. It is probably because the intense GABA_AR α 6 immunoreactivity in the GC layer overshadows the signals in the molecular layer; thus, mGCs have not received much attention. rGCs are densely packed in the GC layer, and they are the most abundant neurons in the mammalian brain. It could

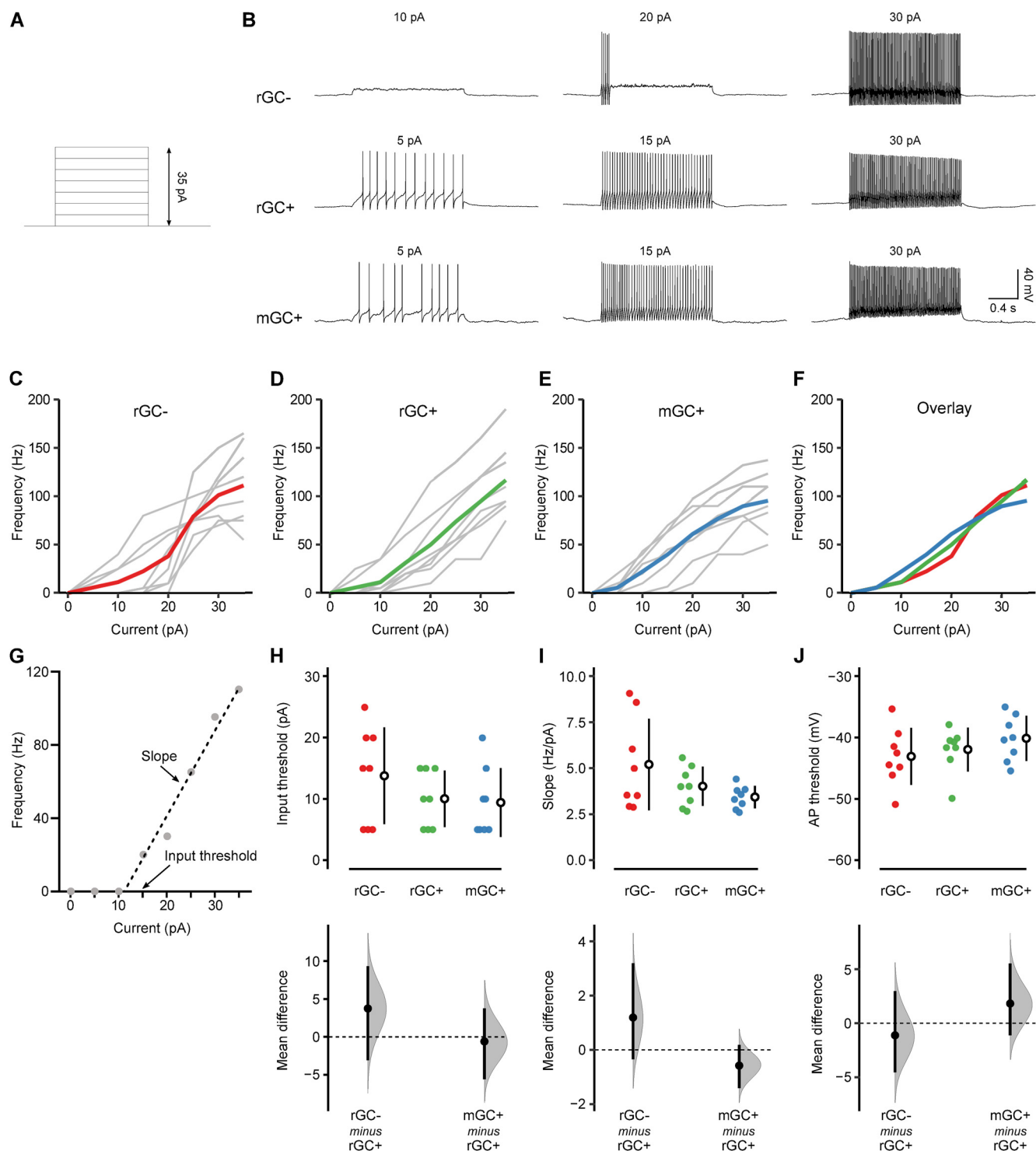


Figure 6. Excitability of mGCs. **A**, Depolarizing current steps (5-pA increment) injected into the cells. **B**, The action potential discharge in a rGC- (top), rGC+ (middle), and mGC+ (bottom) on current injection. The amplitude of the injected current is shown above each trace. **C–E**, The frequency of action potential discharge as a function of injected current in rGC- (**C**), rGC+ (**D**), and mGC+ (**E**). Gray lines represent individual cells, and the colored lines represent the population average. **F**, The population averages of rGC- (red), rGC+ (green), and mGC+ (blue) are overlaid. **G**, A representative current-frequency relationship (gray dots) and the linear regression line (dashed line). The linear fit was performed between the maximum current that did not evoke action potentials (10 pA in this cell) and the current that elicited the highest frequency of action potentials (35 pA in this cell). The input threshold is the minimum current that evoked action potentials (15 pA in this cell). **H–J**, The input threshold (**H**), the slope of the linear regression line (**I**), and action potential threshold (**J**) of rGC- (red; $n=8$), rGC+ (green; $n=8$), and mGC+ (blue; $n=8$) were shown, and the mean differences between rGC+ versus rGC- and rGC+ versus mGC+ were estimated by bootstrap resampling. In the top panels,

continued

the closed circles indicate individual cells. The open circles and vertical lines indicate the mean and SD, respectively. In the bottom panels, the gray curves indicate the resampled distribution of the mean difference between rGC+ versus rGC- (rGC- minus rGC+) and rGC+ versus mGC+ (mGC+ minus rGC+). The closed black circles and vertical lines indicate the observed mean difference and 95% confidence interval, respectively. The horizontal dashed line is the line of zero mean difference.

be possible to argue that mGCs have little contribution to cerebellar function because the fraction of mGCs is small compared with rGCs. However, GC activity is sparse, and only a subset of rGCs convey action potentials to their postsynaptic targets on sensory stimulation (Chadderton et al., 2004; Jörntell and Ekerot, 2006; Ruigrok et al., 2011; Wilms and Häusser, 2015). Therefore, mGC activity might not be overwhelmed by rGCs, and it is more likely the case if mGCs and rGCs receive different types of excitatory inputs.

When we combine all images taken from the entire cerebellum, the mean density of MLIs and mGCs is $110.6 \pm 30.4 \times 10^3/\text{mm}^3$ and $29.4 \pm 14.8 \times 10^3/\text{mm}^3$, respectively. A previous study using Lapham's staining and hematoxylin-eosin staining estimated that the mean density of MLIs was $83.8 \times 10^3/\text{mm}^3$ in mice (Sturrock, 1989), which is reasonably similar to this study. On the other hand, another study using anti-PV antibody estimated that MLI density in mice was $\sim 90/0.1 \text{ mm}^2$ (Collin et al., 2005). If we assume that the density is isotropic, the 2D density of $90/0.1 \text{ mm}^2$ ($900/\text{mm}^2 = 30/\text{mm}$) is converted to the 3D density of $27 \times 10^3/\text{mm}^3$. While this value is substantially smaller than this study and Sturrock, 1989; the accuracy of such conversion is unclear. Besides, obtaining consensus cell density data has been very challenging in general (Keller et al., 2018). Therefore, we argue that the mGC/MLI ratio is more reliable than the absolute density of mGCs and MLIs.

The mGC/MLI ratio was significantly different between the anterior and posterior cerebellum. Although its functional implication is unknown, previous studies also reported other types of difference along the anterior-posterior axis of the cerebellar cortex. For example, a distinct isoform of phospholipase C is used in the anterior and posterior cerebellum for the proper maturation of climbing fiber-Purkinje cell synapses (Kano et al., 1998). Unipolar brush cells, excitatory interneurons in the GC layer, are more prevalent in the posterior cerebellum, particularly in the flocculonodular lobe (Harris et al., 1993; Mugnaini et al., 2011). Still, differences along the anterior-posterior axis are lesser-known than those along the mediolateral axis of the cerebellum (Apps and Hawkes, 2009; Apps et al., 2018). The uneven distribution of mGCs, MLIs, and their ratio reported herein is intriguing because it highlights the heterogeneity of the cerebellar cortex along the anterior-posterior axis.

Developmental profile of mGCs

It was previously speculated that mGCs are the group of GCs that exits the mitotic cycle too late and cannot complete the migration (Berciano and Lafarga, 1988). To test this hypothesis, we performed BrdU cell proliferation assay. Previous studies showed that all GCs are proliferating at P4 (Fujita, 1967), whereas our data showed that

$\sim 50\%$ of rGCs, not 100%, were BrdU-positive when BrdU was injected at P4. This apparent discrepancy is likely because of the frequency of proliferation marker injection. The frequency of injection is critical because the proliferation marker signal gradually decreases and eventually becomes undetectable as the labeled cells undergo more mitotic cycles after injection. We injected BrdU only 1 d in this study; hence even if all GCs were labeled at P4, cells that kept proliferating would eventually be undetectable. On the other hand, previous studies repetitively injected 3H-thymidine over many days until the time of tissue collection at P20 (Fujita, 1967). Therefore, the 3H-thymidine signal was not diluted by proliferation.

To detect GCs that exit the mitotic cycle last, P12 injection should be most efficient because labeled GCs experience fewer mitotic cycles than P4 and P8 injection. However, our data showed that P8 injection was most efficient in labeling mGCs, suggesting that mGCs are not merely the cells that exit the mitotic cycle last. Although it remains unclear why some GCs in the normal cerebellum stop migration in the molecular layer, factors other than timing appear to affect the expression of migratory cue molecules.

rGCs undergo extensive dendritic refinements once they migrate into the GC layer. While immature, postmigration rGCs have >10 dendrites, these nascent dendrites are subsequently pruned such that mature rGCs have an average of four dendrites with claw-like terminals. (Altman, 1972; Dhar et al., 2018). We did not examine whether mGCs also undergo similar dendritic refinements because reconstructing the entire mGC structure is challenging in our specimens because of the parallel fiber labeling (Fig. 4). However, a previous study using Golgi staining showed that mGCs have fewer dendrites than rGCs, and their dendrites often lacked claw-like terminals (Lafarga and Berciano, 1985). These differences might be caused by different presynaptic inputs available in the molecular layer and GC layer.

Motility of mGCs

During the formation of the cerebral cortex, radial glial cells guide the migration of cortical neurons, and they disappear once the migration completes (Gadisseux et al., 1990). On the other hand, Bergmann glia, which guides GC migration in the cerebellum, persistently presents throughout the animals' lives (Yuasa et al., 1996; Dahmane and Ruiz-i-Altaba, 1999; Rahimi-Balaei et al., 2018). Therefore, neuronal migration in the cerebellum might occur beyond the developmental period. Indeed, a relatively recent study suggested that neuronal proliferation and migration in the rabbit cerebellum continue until around six months old, much later than the disappearance of the external GC layer around five weeks old (Ponti et al., 2008). Traditionally, GC

migration has been thought to be complete by the end of the third postnatal week in rats and mice (Altman and Bayer, 1996; Rahimi-Balaei et al., 2018). However, a small number of late migrating GCs, even if they exist, are difficult to detect by between-animal comparisons of fixed tissues. To examine whether mGCs are on their way to the GC layer or stay in the molecular layer, we performed two-photon imaging and followed the same mGCs for days to months *in vivo*. Our data demonstrated that mGCs are not migrating. Thus, mGCs stay in the molecular layer despite the persistent presence of Bergmann glia.

Physiologic properties of mGCs and comparison to other ectopic neurons

While previous studies analyzed the electrophysiological properties of immature GCs before or during the migration in the molecular layer, no functional characterization has yet been made for mGCs in the adult cerebellum. We took advantage of GC-specific labeling in TCGO mice and performed the first-ever electrophysiological recordings from mGCs. One of the most significant findings is that the intrinsic membrane properties of mGCs are as mature as rGCs. In particular, the capability of mGCs to discharge action potentials is crucial because it allows them to be a part of synaptic circuits in the cerebellar cortex.

One unexpected finding is that some physiological properties of mGCs were more homogenous than rGCs as shown by less variation within the group. It may suggest that the functional maturation of individual GCs is influenced by cell-to-cell variation in their developmental process occurring in the GC layer, such as the pruning of excess dendrites. Another interesting observation is that mCitrine-nonexpressing rGCs (rGC⁻) tend to show slightly different membrane properties and excitabilities from mCitrine-expressing rGCs (rGC⁺) and mGCs (mGC⁺). Although the difference was not statistically significant, mCitrine expression might affect the physiological properties of GCs to some extent. Alternatively, mCitrine expression in TCGO mice might not be random but specific to a previously unknown GC subgroup.

Ectopic neurons that have been most extensively studied thus far are GCs in the hippocampal dentate gyrus (DG). Regular DG GCs reside in the GC layer and extend their dendrites in the molecular layer, where they receive excitatory inputs from the perforant path. They send their axons, mossy fibers, toward CA3 regions through the hilus. However, a small population of DG GCs resides in the hilus in normal animals, and the population increases substantially after a seizure (Gaarskjaer and Laurberg, 1983; Parent et al., 1997; Scharfman et al., 2007). Depending on the proximity to the GC layer, those hilar ectopic GCs have their dendrite in the molecular layer or not (Scharfman et al., 2007; Pierce et al., 2011).

Hilar ectopic GCs in the normal animals showed similar intrinsic membrane properties as regular DG GCs (Scharfman et al., 2003, 2007), which is consistent with mGCs in this study. Although little is known about the synaptic connectivity of hilar ectopic GCs in the normal DG, seizure-induced hilar ectopic GCs receive excitatory inputs from mossy fibers,

suggesting that they receive primary inputs from other GCs (Pierce et al., 2005).

In the cerebellum, rGCs receive excitatory inputs from mossy fibers (the same name but different from the hippocampal mossy fibers) in the GC layer. Since cerebellar mossy fibers rarely innervate into the molecular layer, we argue that the amount of mGCs seems too many if all of them are innervated by mossy fibers. Indeed, mGC clusters near the pia mater make synapses with mossy fibers, whereas individual mGCs dispersed in the molecular layer do not (Lafarga and Berciano, 1985). Perhaps, individual GCs cannot produce sufficiently strong neurotropic cues to attract mossy fibers.

If mGCs are innervated by nearby axon terminals in the molecular layer, two potential sources of inputs are parallel fibers and climbing fibers (Palay and Chan-Palay, 1974; Altman and Bayer, 1996). Parallel fibers are the axons of rGCs. If mGCs receive parallel fiber inputs, they receive inputs from other GCs, which somewhat resemble seizure-induced hilar ectopic GCs in the hippocampal DG.

Climbing fibers release a massive amount of glutamate, evoking EPSCs via spillover in nearby cells even if they are not synaptically connected. All previously examined neurons and glial cells, whose dendrites or processes reside in the molecular layer, receive climbing fiber inputs via synaptic transmission or spillover (Matsui and Jahr, 2003, 2004; Lin et al., 2005; Szapiro and Barbour, 2007; Coddington et al., 2013; Nietz et al., 2017). Therefore, it is hard to imagine that only mGCs are somehow sequestered from the spillover-mediated volume transmission in the molecular layer. Identifying presynaptic inputs of mGCs is the next crucial step for understanding their potential roles in cerebellar synaptic circuitry.

References

- Altman J (1972) Postnatal development of the cerebellar cortex in the rat. 3. Maturation of the components of the granular layer. *J Comp Neurol* 145:465–513.
- Altman J, Bayer SA (1996) Development of the cerebellar system: in relation to its evolution, structure, and functions, Ed 1. Boca Raton: CRC-Press.
- Apps R, Hawkes R (2009) Cerebellar cortical organization: a one-map hypothesis. *Nat Rev Neurosci* 10:670–681.
- Apps R, Hawkes R, Aoki S, Bengtsson F, Brown AM, Chen G, Ebner TJ, Isope P, Jörntell H, Lackey EP, Lawrenson C, Lumb B, Schonewille M, Sillitoe RV, Spaeth L, Sugihara I, Valera A, Voogd J, Wylie DR, Ruigrok TJH (2018) Cerebellar modules and their role as operational cerebellar processing units. *Cerebellum* 17:654–682.
- Bastianelli E (2003) Distribution of calcium-binding proteins in the cerebellum. *Cerebellum* 2:242–262.
- Berciano MT, Lafarga M (1988) Colony-forming ectopic granule cells in the cerebellar primary fissure of normal adult rats: a morphologic and morphometric study. *Brain Res* 439:169–178.
- Brandalise F, Lujan R, Leone R, Lodola F, Cesaroni V, Romano C, Gerber U, Rossi P (2016) Distinct expression patterns of inwardly rectifying potassium currents in developing cerebellar granule cells of the hemispheres and the vermis. *Eur J Neurosci* 43:1460–1473.
- Brzustowicz RJ, Kernohan JW (1952) Cell rests in the region of the fourth ventricle: II. Histologic and embryologic consideration. *AMA Arch Neurol Psychiatry* 67:592–601.

- Calin-Jageman RJ, Cumming G (2019) Estimation for better inference in neuroscience. *eNeuro* 6:ENEURO.0205-19.2019.
- Chadderton P, Margrie TW, Häusser M (2004) Integration of quanta in cerebellar granule cells during sensory processing. *Nature* 428:856–860.
- Chan-Palay V (1972) Arrested granule cells and their synapses with mossy fibers in the molecular layer of the cerebellar cortex. *Z Anat Entwicklungsgesch* 139:11–20.
- Coddington LT, Rudolph S, Vande Lune P, Overstreet-Wadiche L, Wadiche JI (2013) Spillover-mediated feedforward inhibition functionally segregates interneuron activity. *Neuron* 78:1050–1062.
- Collin T, Chat M, Lucas MG, Moreno H, Racay P, Schwaller B, Marty A, Llano I (2005) Developmental changes in parvalbumin regulate presynaptic Ca²⁺ signaling. *J Neurosci* 25:96–107.
- Dahmane N, Ruiz-i-Altaba A (1999) Sonic hedgehog regulates the growth and patterning of the cerebellum. *Development* 126:3089–3100.
- D'Angelo E (2018) Chapter 6 - Physiology of the cerebellum. In: *Handbook of clinical neurology, the cerebellum: from embryology to diagnostic investigations* (Manto M, Huisman TAGM eds), pp 85–108. San Diego: Elsevier.
- Dhar M, Hantman AW, Nishiyama H (2018) Developmental pattern and structural factors of dendritic survival in cerebellar granule cells in vivo. *Sci Rep* 8:17561.
- Fortin M, Marchand R, Parent A (1998) Calcium-binding proteins in primate cerebellum. *Neurosci Res* 30:155–168.
- Fujita S (1967) Quantitative analysis of cell proliferation and differentiation in the cortex of the postnatal mouse cerebellum. *J Cell Biol* 32:277–287.
- Gaarskjaer FB, Laurberg S (1983) Ectopic granule cells of hilus fasciae dentatae projecting to the ipsilateral regio inferior of the rat hippocampus. *Brain Res* 274:11–16.
- Gadisseux JF, Kadhim HJ, van den Bosch de Aguilar P, Caviness VS, Evrard P (1990) Neuron migration within the radial glial fiber system of the developing murine cerebrum: an electron microscopic autoradiographic analysis. *Brain Res Dev Brain Res* 52:39–56.
- Harris J, Moreno S, Shaw G, Mugnaini E (1993) Unusual neurofilament composition in cerebellar unipolar brush neurons. *J Neurocytol* 22:1039–1059.
- Ho J, Tumkaya T, Aryal S, Choi H, Claridge-Chang A (2019) Moving beyond P values: data analysis with estimation graphics. *Nat Methods* 16:565–566.
- Huang CC, Sugino K, Shima Y, Guo C, Bai S, Mensh BD, Nelson SB, Hantman AW (2013) Convergence of pontine and proprioceptive streams onto multimodal cerebellar granule cells. *Elife* 2:e00400.
- Jörntell H, Ekerot CF (2006) Properties of somatosensory synaptic integration in cerebellar granule cells in vivo. *J Neurosci* 26:11786–11797.
- Kadowaki K, McGowan E, Mock G, Chandler S, Emson PC (1993) Distribution of calcium binding protein mRNAs in rat cerebellar cortex. *Neurosci Lett* 153:80–84.
- Kalinichenko SG, Pushchin II (2008) Calcium-binding proteins in the cerebellar cortex of the bottlenose dolphin and harbour porpoise. *J Chem Neuroanat* 35:364–370.
- Kamiya S, Sawada K (2021) Immunohistochemical characterization of postnatal changes in cerebellar cortical cytoarchitectures in ferrets. *Anat Rec (Hoboken)* 304:413–424.
- Kano M, Hashimoto K, Watanabe M, Kurihara H, Offermanns S, Jiang H, Wu Y, Jun K, Shin HS, Inoue Y, Simon MI, Wu D (1998) Phospholipase cbeta4 is specifically involved in climbing fiber synapse elimination in the developing cerebellum. *Proc Natl Acad Sci USA* 95:15724–15729.
- Kato K (1990) Novel GABAA receptor α subunit is expressed only in cerebellar granule cells. *J Mol Biol* 214:619–624.
- Keller D, Erö C, Markram H (2018) Cell densities in the mouse brain: a systematic review. *Front Neuroanat* 12:83.
- Lafarga M, Berciano MT (1985) A Golgi and morphometric study of the ectopic granule cells in the molecular layer of the rat cerebellum. *Brain Res* 345:398–401.
- Laurie D, Wisden W, Seeburg P (1992a) The distribution of thirteen GABAA receptor subunit mRNAs in the rat brain. III. Embryonic and postnatal development. *J Neurosci* 12:4151–4172.
- Laurie DJ, Seeburg PH, Wisden W (1992b) The distribution of 13 GABAA receptor subunit mRNAs in the rat brain. II. Olfactory bulb and cerebellum. *J Neurosci* 12:1063–1076.
- Levine JM, Card JP (1987) Light and electron microscopic localization of a cell surface antigen (NG2) in the rat cerebellum: association with smooth protoplasmic astrocytes. *J Neurosci* 7:2711–2720.
- Lin SC, Huck JHJ, Roberts JDB, Macklin WB, Somogyi P, Bergles DE (2005) Climbing fiber innervation of NG2-expressing glia in the mammalian cerebellum. *Neuron* 46:773–785.
- Matsui K, Jahr CE (2003) Ectopic release of synaptic vesicles. *Neuron* 40:1173–1183.
- Matsui K, Jahr CE (2004) Differential control of synaptic and ectopic vesicular release of glutamate. *J Neurosci* 24:8932–8939.
- McCloskey DP, Hintz TM, Pierce JP, Scharfman HE (2006) Stereological methods reveal the robust size and stability of ectopic hilar granule cells after pilocarpine-induced status epilepticus in the adult rat. *Eur J Neurosci* 24:2203–2210.
- Mellor JR, Merlo D, Jones A, Wisden W, Randall AD (1998) Mouse cerebellar granule cell differentiation: electrical activity regulates the GABAA receptor alpha 6 subunit gene. *J Neurosci* 18:2822–2833.
- Mugnaini E, Sekerková G, Martina M (2011) The unipolar brush cell: a remarkable neuron finally receiving deserved attention. *Brain Res Rev* 66:220–245.
- Nietz AK, Vaden JH, Coddington LT, Overstreet-Wadiche L, Wadiche JI (2017) Non-synaptic signaling from cerebellar climbing fibers modulates Golgi cell activity. *Elife* 6:e29215.
- Nishiyama N, Colonna J, Shen E, Carrillo J, Nishiyama H (2014) Long-term in vivo time-lapse imaging of synapse development and plasticity in the cerebellum. *J Neurophysiol* 111:208–216.
- Nusser Z, Sieghart W, Stephenson FA, Somogyi P (1996) The alpha 6 subunit of the GABAA receptor is concentrated in both inhibitory and excitatory synapses on cerebellar granule cells. *J Neurosci* 16:103–114.
- Ohshima T, Endo T, Onaya T (1991) Distribution of parvalbumin immunoreactivity in the human brain. *J Neurol* 238:320–322.
- Palay SL, Chan-Palay V (1974) *Cerebellar cortex: cytology and organization*. New York: Springer.
- Parent JM, Yu TW, Leibowitz RT, Geschwind DH, Sloviter RS, Lowenstein DH (1997) Dentate granule cell neurogenesis is increased by seizures and contributes to aberrant network reorganization in the adult rat hippocampus. *J Neurosci* 17:3727–3738.
- Pierce JP, Melton J, Punsoni M, McCloskey DP, Scharfman HE (2005) Mossy fibers are the primary source of afferent input to ectopic granule cells that are born after pilocarpine-induced seizures. *Exp Neurol* 196:316–331.
- Pierce JP, McCloskey DP, Scharfman HE (2011) Morphometry of hilar ectopic granule cells in the rat. *J Comp Neurol* 519:1196–1218.
- Ponti G, Peretto P, Bonfanti L (2008) Genesis of neuronal and glial progenitors in the cerebellar cortex of peripuberal and adult rabbits. *PLoS One* 3:e2366.
- Rahimi-Balaei M, Bergen H, Kong J, Marzban H (2018) Neuronal migration during development of the cerebellum. *Front Cell Neurosci* 12:484.
- Ruigrok TJH, Hensbroek RA, Simpson JI (2011) Spontaneous activity signatures of morphologically identified interneurons in the vestibulocerebellum. *J Neurosci* 31:712–724.
- Scharfman HE, Sollas AE, Berger RE, Goodman JH, Pierce JP (2003) Perforant path activation of ectopic granule cells that are born after pilocarpine-induced seizures. *Neuroscience* 121:1017–1029.
- Scharfman H, Goodman J, McCloskey D (2007) Ectopic granule cells of the rat dentate gyrus. *Dev Neurosci* 29:14–27.

- Shima Y, Sugino K, Hempel CM, Shima M, Taneja P, Bullis JB, Mehta S, Lois C, Nelson SB (2016) A Mammalian enhancer trap resource for discovering and manipulating neuronal cell types. *Elife* 5:e13503.
- Spacek J, Parížek J, Lieberman AR (1973) Golgi cells, granule cells and synaptic glomeruli in the molecular layer of the rabbit cerebellar cortex. *J Neurocytol* 2:407–428.
- Sturrock RR (1989) Changes in neuron number in the cerebellar cortex of the ageing mouse. *J Hirnforsch* 30:499–503.
- Szapiro G, Barbour B (2007) Multiple climbing fibers signal to molecular layer interneurons exclusively via glutamate spillover. *Nat Neurosci* 10:735–742.
- Takao M, Ghetti B, Murrell JR, Unverzagt FW, Giaccone G, Tagliavini F, Bugiani O, Piccardo P, Hulette CM, Crain BJ, Farlow MR, Heyman A (2001) Ectopic white matter neurons, a developmental abnormality that may be caused by the PSEN1 S169L mutation in a case of familial AD with myoclonus and seizures. *J Neuropathol Exp Neurol* 60:1137–1152.
- Watrín F, Manent J-B, Cardoso C, Represa A (2015) Causes and consequences of gray matter heterotopia. *CNS Neurosci Ther* 21:112–122.
- Wilms CD, Häusser M (2015) Reading out a spatiotemporal population code by imaging neighbouring parallel fibre axons in vivo. *Nat Commun* 6:6464.
- Yuasa S, Kawamura K, Kuwano R, Ono K (1996) Neuron-glia interrelations during migration of Purkinje cells in the mouse embryonic cerebellum. *Int J Dev Neurosci* 14:429–438.